University of BRISTOL

Fiat 595 Abarth Convertible Roof Technical Analysis

Group Members: Darian Irani (en20703), Viral Shah (di20467), Andhika Nasution (ei20239)

Group 1a

Report date: 06/05/2022

Abstract

The assignment was to design a convertible roof mechanism for the Fiat 595 Abarth with an aim to put it in direct competition with the BMW Mini Cooper convertible. This report aimed to test the feasibility of a proof of concept, with the goal of mass production. Through the several stages of the project, concepts were rigorously assessed prioritising cost and safety and maintaining level performance. Combining technical analysis with thorough mechanical design, it was decided that this system would be developed and taken forward to the engineering team at Abarth.

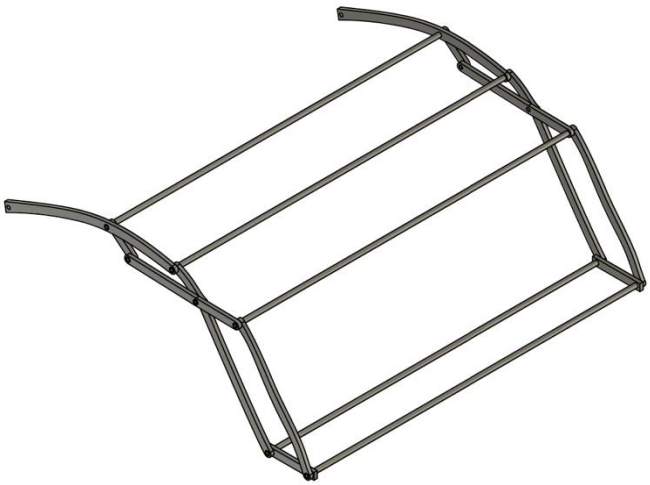

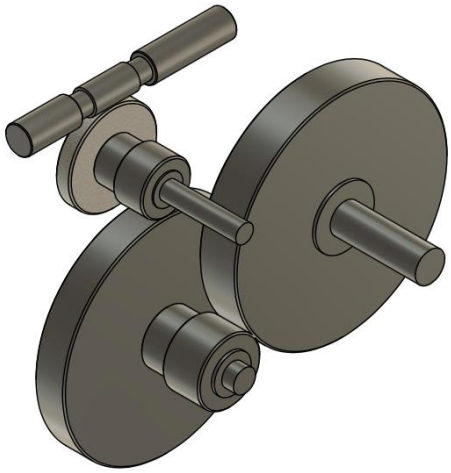

TA1. Initial Model

Note: All figures in this report were produced using the 'NSA-I 0 390 204 166' motor with a gear ratio of 400. This was purely arbitrary and kept constant so outputs could be tracked and compared as input parameters changed and developed.

The fundamental model of the roof was based on a single-degree-of-freedom rotating inverted pendulum, shown in Fig. 1. The mass of the mechanism was assumed to be a point at the end of a rod, which itself was modelled as light and rigid. The reason why this modelling assumption was fair is due to how the system rotates about a fixed pivot - mirroring the motion of a pendulum. The other option was to consider all members and the canvas as uniformly distributed loads, which while more realistic, would not be feasible given the complexity of the dynamics of the system. The motion was expressed using Newton's second law, as seen in (1). Other assumptions included the mass of the system and radius of the centre of mass – 20kg & 0.37m.

Table 1: Table showing assumptions, inaccuracies, and mitigations

Assumption	Innacuracy	Mitigation
Radius of centre of mass is fixed	Dynamics system hence centre of mass constantly changing	Variable radius for C.O.M added
Negligible force from headwind	This force would accelerate retraction and decelerate deployment	Aerodynamic force due to 20mph headwind added, with estimation of C_d

$$T_a - T_r = I\ddot{\theta} \tag{1}$$

where the moment of inertia [1] $I = mr^2$ [kgm^2]; $\ddot{\theta}$ is the angular acceleration [rads^{-2}]; T_a are the accelerating torques and T_r are the resistive torques [Nm].

To solve the differential equation presented in (1), the model used MATLAB's ode45 function, from an initial angle of 4.19 to 1.98 radians, with position and angular speed outputs. Measuring from the positive x-axis, the initial angle is 2.62 radians, however $\frac{1}{2}\pi$ had to be added from MATLAB's datum of the negative y-axis. The base model had only two torques acting on it: the motor as an accelerating torque (clockwise/anticlockwise for retraction/deployment) and gravity as a decelerating torque. These equations can be found in Appendix A.

Using this initial model, the results showed that the retraction time was 2.48s, as depicted in Fig. 3 which is not feasible nor realistic. The motion was rather slow initially, when working against gravity, then very quick for the second half with gravity aiding the system. The takeaways from this model were that the operation time needed to be increased, along with a smoother and more consistent motion. These inaccuracies were consequences of initial assumptions to the model, which are presented in Table 1. The analysis process from the model was an iterative one, using the outputs of each model version to build and improve upon the next. The process can be outlined with a flowchart, seen below in Fig. 2.

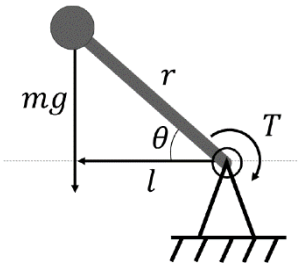

Figure 1: FBD of mechanism modelled as inverted pendulum [3]

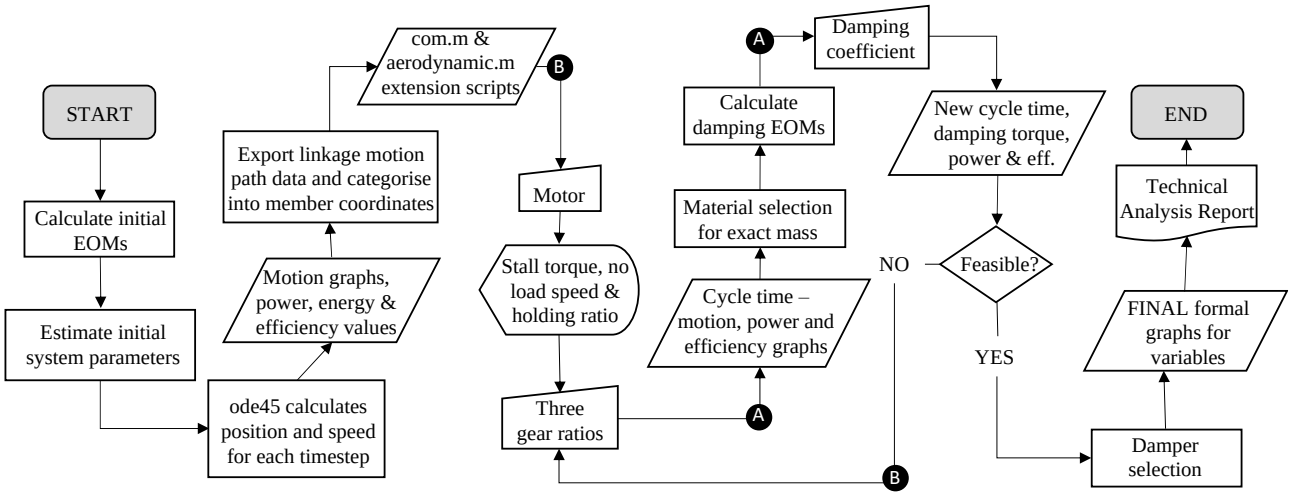

Figure 2: Flowchart of how model was used for analysis and mechanical design iterations

TA2. Modelling Extensions

TA2.1 Variable Radius of Centre of Mass (COM)

As a mitigation to initial assumptions, a variable radius of COM was implemented. 652 motion-path data points were extracted from Linkage, processed in a spreadsheet, and using (2) and (3) the radius for the COM was found for each timestep. At this stage, mass was unknown however density was assumed constant, and hence mass was replaced with length, due to proportionality, as depicted in (2) and (3).

$$X_{CoM} = \frac{\sum_{i=1}^{N} l_i X_i}{L} \qquad (2) \qquad Y_{CoM} = \frac{\sum_{i=1}^{N} l_i Y_i}{L} \qquad (3)$$

where N is the number of members; l is the length of each member [m]; L is the total length per timestep and (X, Y) are the midpoints of each member.

From the data, every value of radius had a corresponding value of theta. This was used in a simple lookup script that would compare the output angle from the ode45 function, against the values in the spreadsheet to a specific tolerance, and then choosing the subsequent radius. The new cycle time was 2.5s, as depicted in Fig. 3. Although not a significant difference, this new model is more accurate and reflective of real practises.

TA2.2 Aerodynamic Resistance

Variable aerodynamic force of 20mph oncoming wind was modelled onto the mechanism as per Requirement 6. This was to ensure that Requirement 11 could still be met even under these conditions. Beyond 20mph, the mechanism was programmed to terminate (as detailed in the Mechatronics Report). Equation (4) represents the aerodynamic force, whilst (5) represents the aerodynamic torque acting at a radius (assumed to be the same as COM). Other assumptions also included: Laminar, incompressible and 1D flow since turbulent flow would not be feasible to include within the model; effects of flow from contact with the windshield are negligible as again, this would result in non-uniform components acting on the specified area as well as turbulence from flow travelling over the windscreen and into the car; effects of lateral/angular flow not considered – only incoming flow perpendicular to the car considered. Table 2 shows constants used in (4).

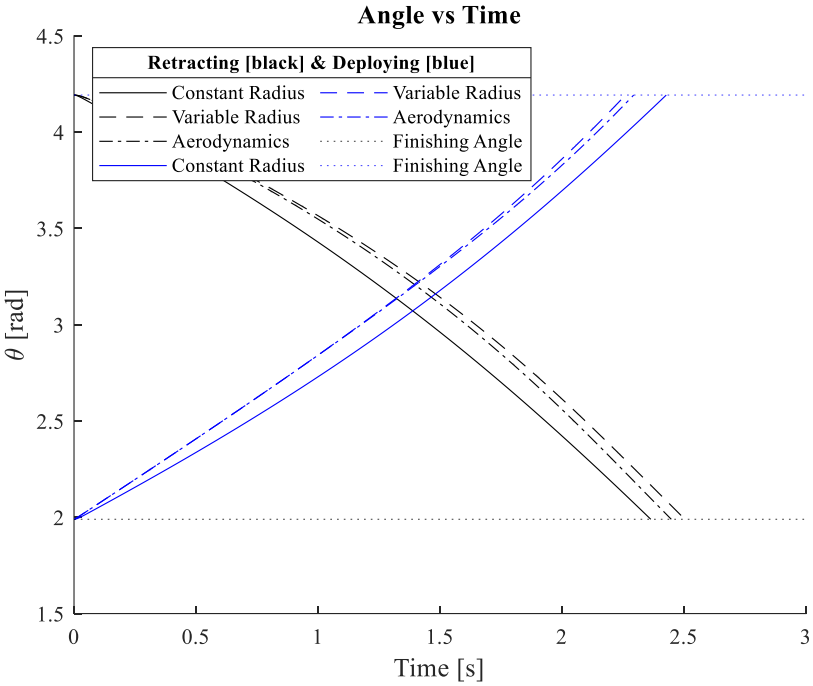

Figure 3: Graphs showing retracting and deploying operation time for constant, variable radius, and aerodynamic resistance

$$F_{aero} = \rho v^2 C_d y w / 2 \qquad (4) \qquad T_{aero} = F_{aero} r \qquad (5)$$

where ρ is the density of air [kgm^{-3}]; v is the wind velocity [ms^{-2}]; w is the width of the car = 1.204m; y is the swept height of the roof [m]; C_d is the drag coefficient and r is the radius of centre of mass [m].

Table 2: Constants used in Equation (4) with explanations and magnitudes

Variable	Value	Explanation
ρ	1.225	Density of air at sea level
C_d	2.05	Drag coefficient for a rectangular prism

The swept heights at each timestep were calculated as the difference between the highest joint and the top of the windshield (see D3.1 Fig. 3). The same lookup script from TA2.1. selected this value for each angle. Finally, airflow was modelled to contact the frontal surface of a rectangular prism for C_d [2] .At first, this was modelled as a flat plate however this assumes negligible thickness and doesn't consider the length of the roof.

Due to the streamlined mechanism design, the swept height remains low throughout the motion, hence not causing significant drag forces. These effects are portrayed by the dash-dotted curves in Fig.3, where deployment is slower and retraction is faster, as intended.

TA2.3 Damping

As seen in Fig. 3, the cycle time was far too quick, as well as the rate of change of angle turned out to be too fast. The curve is shallow in the first half as the mechanism is overcoming the resistance of gravity, whereas the latter half is very steep due to gravity aiding the mechanism. Aside from adding to the realism of the model, the main reasons for including damping were to: increase cycle time by slowing the system velocity; attain a smoother, more consistent motion and lastly, to provide extra safety by preventing damage from rapid acceleration at the end. Two forms of dampers were considered – linear and rotational.

Firstly, linear extension dampers were considered and configured as outlined in D5.1. modelled using (6). This was implemented by keeping the damping force non-zero for the angles at which extension occurred, and zero for the rest of the motion – the transition angle being found through the physical model. This was to counteract the gravitational acceleration in the second half of motion for both cycles. As observed in Fig. 4 there is a sudden change in speed when damping begins. Although this shock was expected and would be absorbed by the damper, over time this would lead to more frequent replacements due to the extra stress. The results showed that even the highest available damping coefficient offered only a 0.43s increase in cycle time.

$$T_{LD} = c_1 \omega r_d^2 \qquad (6) \qquad\qquad T_{CRD} = c_2 \omega \qquad (7)$$

where c_1, c_2 are damping coefficients [Nsm^{-1}, Nmsrad^{-1}]; ω is angular velocity [rads^{-1}] and r_d is the radius of the arc created by the connecting rod [m].

Next, to mitigate the shock, a dual-direction linear damper of the highest coefficient was used. This means that a damping torque was exerted on the mechanism in both extension and compression. Referring to Fig. 4, the first half of the motion also being dampened helps to further increase cycle time.

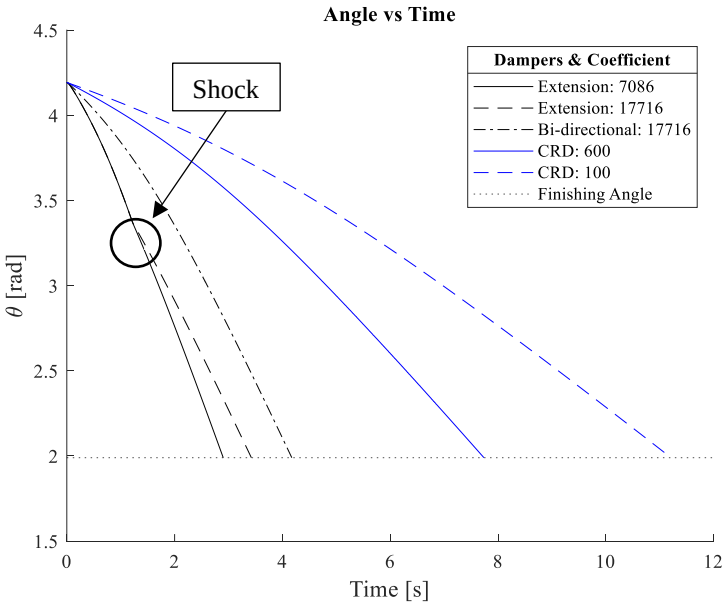

Figure 4: Graphs showing retracting and deploying operation time for constant, variable radius, and aerodynamic resistance

The main loss of damping torque was due to both linear velocity and the connecting rod combining for a factor of r_d^2, totalling an effect of magnitude 10^{-4}. To eliminate this distance, a continuous rotational damper (CRD) was used as detailed in D5.2. and modelled using (7). Multiple, arbitrary damping coefficients were tested as shown in Fig. 4 and it can be noted that even the lowest tested coefficient gives almost double the operation time as the dual-direction linear damper. This partially resulted in choosing CRDs over linear dampers, with other reasons being highlighted in D5.3.

TA2.4 Snow

As an extreme scenario, the roof may be attempted to be opened with a large weight of snow collected upon it. In this case, the total mass of the snow would be considered to incorporate with the COM of the mechanism. Although not an accurate assumption, this was more feasible than including the snow as a uniformly distributed load within the model. Through iteration, it was found that the roof would maintain cycle time within the stated boundaries of Requirement 11 in the PDS, with up to 11.26kg of snow on it. This is also shown in D6.3 Fig. 17. This was tested after the final parameters for the model had been selected.

References

[1] R. Nave, “Hyperphysics Mechanics Rotation,” [Online]. Available: http://hyperphysics.phy-astr.gsu.edu/hbase/mi.html#:~:text=For%20a%20point%20mass%2C%20the,a%20collection%20of%20point%20masses..

[2] e. a. Baker, Table 2-2 Drag coefficient for various object shapes, 1983.

[3] Snider, C., 2022. Engineering Practice Summative Project 2022.

Appendix

Equations:

$$T_a = T_{motor} = -\left(\frac{T_{stall}}{\omega_{no\ load}}\right)\omega_{motor} + T_{stall} \quad [A]$$

$$T_r = T_{gravity} = -mgr\cos(\theta - \pi/2) \quad [B]$$

where T_{stall} is the torque at zero angular velocity [Nm]; $\omega_{no\ load}$ is the angular velocity at zero torque and ω_{motor} is the angular speed of the motor [rads^{-1}]; m is the mass of the mechanism [kg]; g is acceleration due to gravity [ms^{-2}]; r is the radius of the centre of mass [m] and θ is the angle of the mechanism [rad].